Supplementary data

Flexible hand-made carbon electrode decorated with metronidazole imprinted polymer

Dominik Korol,*[,a] Kostiantyn Nikiforow,[a] Paweł Borowicz,[a]
Piyush Sindhu Sharma[a] and Maciej Cieplak[a,*]

[a] *Institute of Physical Chemistry of the Polish Academy of Sciences, Kasprzaka 44/52, 01-224 Warsaw, Poland*

Corresponding Authors

Dominik Korol: dkorol@ichf.edu.pl

Maciej Cieplak: mcieplak@ichf.edu.pl

S1. Reproducibility of the analytical signal at flexible carbon paper-based electrodes

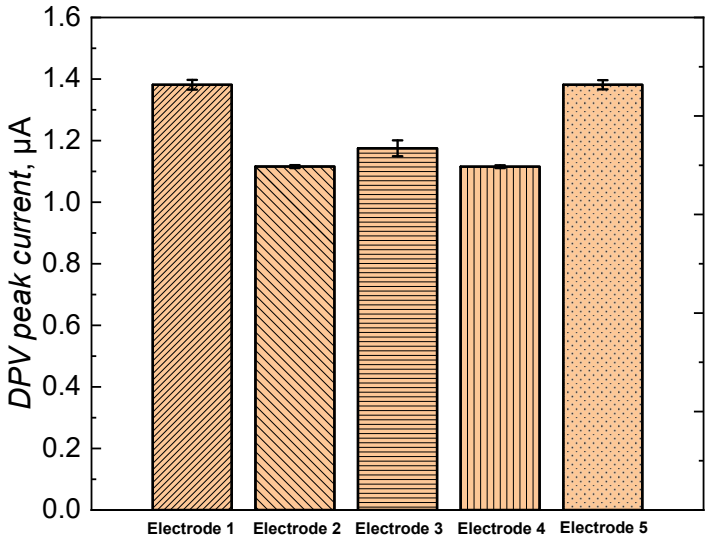

Figure S1. A bar chart showing the DPV peak currents recorded over five independently fabricated bare carbon paper electrodes. The DPV measurement was recorded in an aqueous solution containing 1 mM $Ru(NH_3)_6Cl_3$ in 0.1 M KCl.

S2. Electrochemical characterization of metronidazole and functional monomers

To characterize the electrochemical properties of **MTZ**, DPV was performed in the presence of 200 nM **MTZ** in 0.1 M solution of KCl (Figure S2). No signal originating from the faradaic process was observed, proving that **MTZ** is non-electroactive in the potential range of −0.4 to 0.0 V vs. Ag quasi-reference electrode.

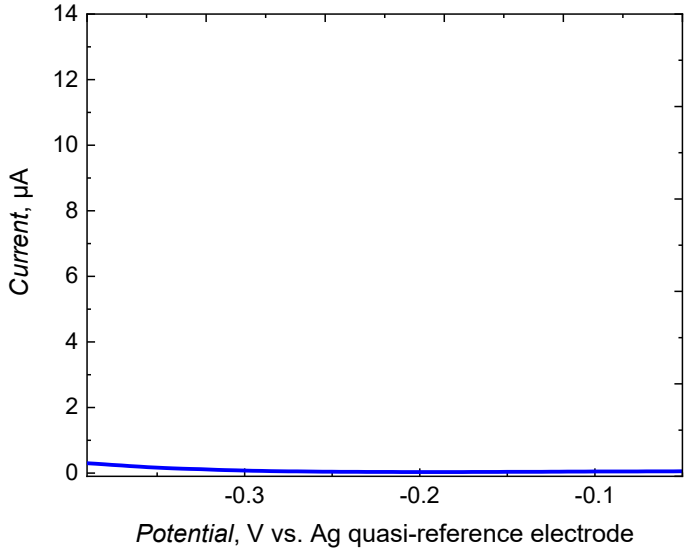

Figure S2. DPV curves recorded in 200 nM **MTZ** solution in 0.1 M $KCl_{(aq)}$ on the unmodified carbon paper electrode.

The electrochemical properties of pyrrole derivatives differ from pristine pyrrole. For this reason, chronocoulometric curves of Py and **Py-COOH** galvanostatic polymerization were recorded (Figure S3).

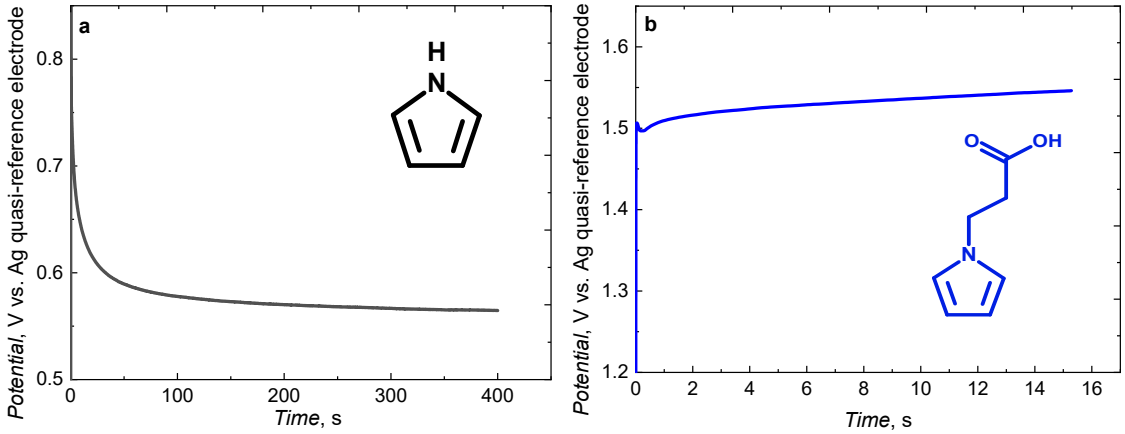

Figure S3. Chronocoulometric curves recorded during galvanostatic electropolymerization of (a) 0.1 M Py and (b) 1 mM **Py-COOH** in 1.0 M KCl/H_2O, at the constant current appliance of 200 µA, and charge of (a) 80 mC and (b) 3 mC.

Another pyrrole derivative – 3-(1*H*-pyrrol-1-yl)propanamine (**Py-NH_2**) could have been tried as a functional monomer; however, polymerization of this monomer on the surface of the gold electrode (Figure S4a) resulted in a polymer of low conductivity. This film completely blocked the electrode surface (Figure S4b). Because of this reason, **Py-NH_2** was not used as a functional monomer for further studies.

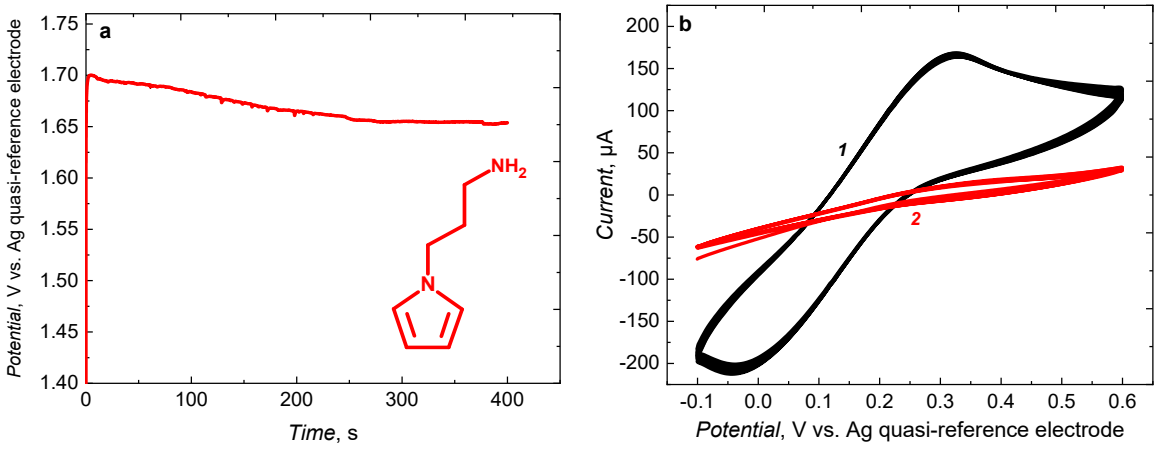

Figure S4. (a) Chronocoulometric curves recorded during galvanostatic electropolymerization of 1 mM **Py-NH_2** in 1.0 M $KCl_{(aq)}$, 200 µA, 80 mC. (b) Multicyclic voltammetric curves recorded in a redox probe (10 mM $K_3[Fe(CN)_6]$, and 10 mM $K_4[Fe(CN)_6]$ in aqueous PBS buffer), for (*1*) a carbon paper electrode and (*2*) a carbon paper electrode coated with a poly(**Py-NH_2**) obtained after **Py-NH_2** polymerization.

S3. Extraction of MIP and NIP films

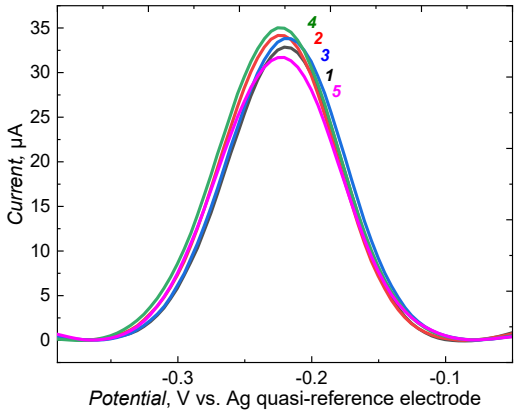

Figure S5. DPV curves recorded in 5 mM $Ru(NH_3)_6Cl_3$ solution in 0.1 M $KCl_{(aq)}$ on the MIP film-coated electrode (*1*) after electrodeposition or after (*2*) 15 min, (*3*) 30 min, (*4*) 60 min, and (*5*) 90 min extraction in 1mM $HCl_{(aq)}$.

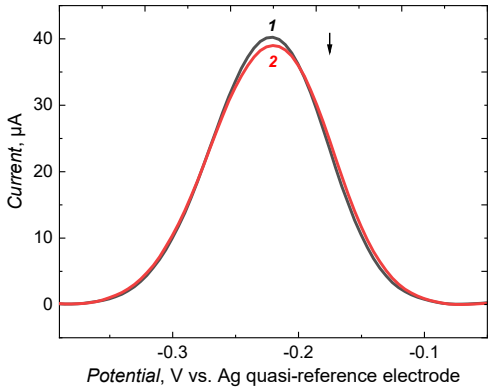

Figure S6. DPV curves recorded in 5 mM $Ru(NH_3)_6Cl_3$ solution in 0.1 M $KCl_{(aq)}$ on the NIP film-coated electrode (*1*) after electrodeposition and after (*2*) 60 min extraction in 0.1 M carbonate buffer of pH = 9.1.

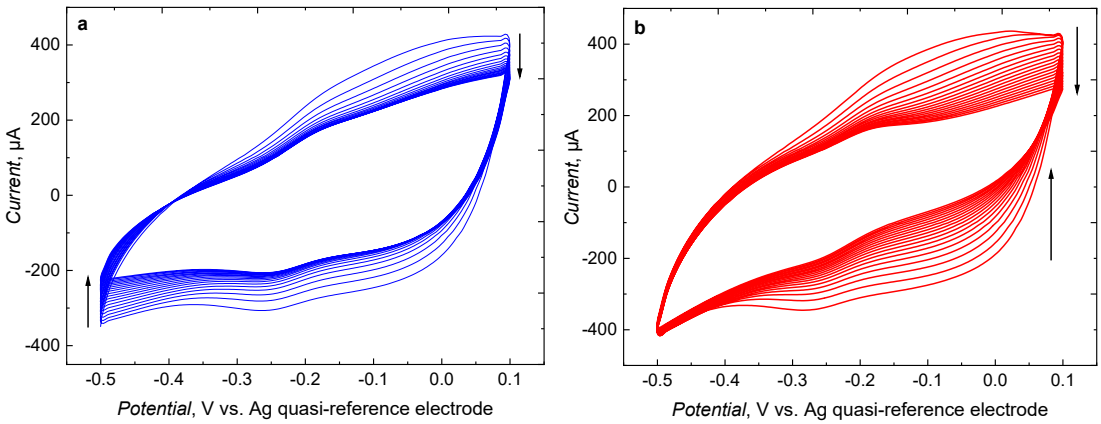

Figure S7. CV curves recorded in 1 mM $Ru(NH_3)_6Cl_3$ solution in 0.1 M $KCl_{(aq)}$ on the (a) MIP and (b) NIP film-coated electrode after 60 min extraction in 0.1 M carbonate buffer of pH = 9.1.

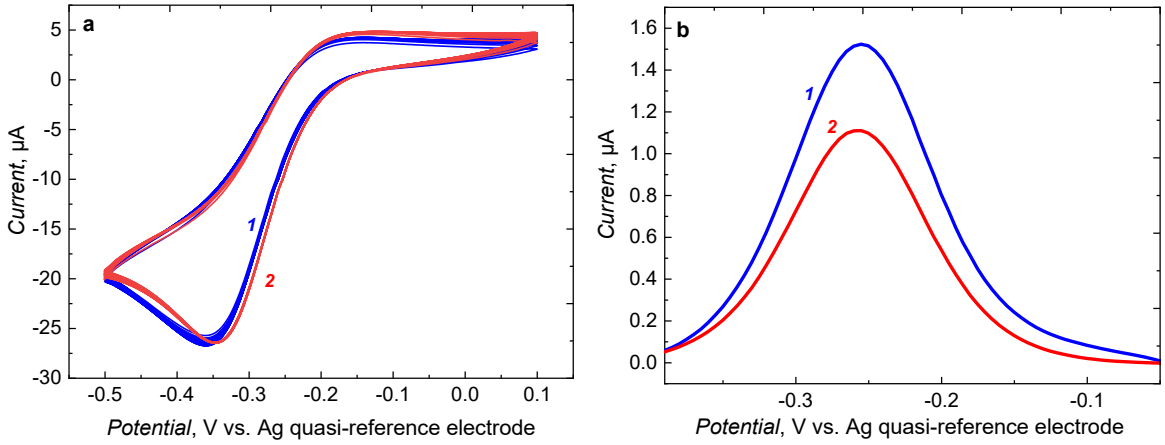

Figure S8. (a) CV and (b) DPV curves recorded in 1 mM $Ru(NH_3)_6Cl_3$ solution in 0.1 M $KCl_{(aq)}$ on the pristine carbon paper electrode (*1*) before and (*2*) after 60 min treatment with 0.1 M carbonate buffer of pH = 9.1.

S4. SEM imaging of the deposited MIP and NIP films

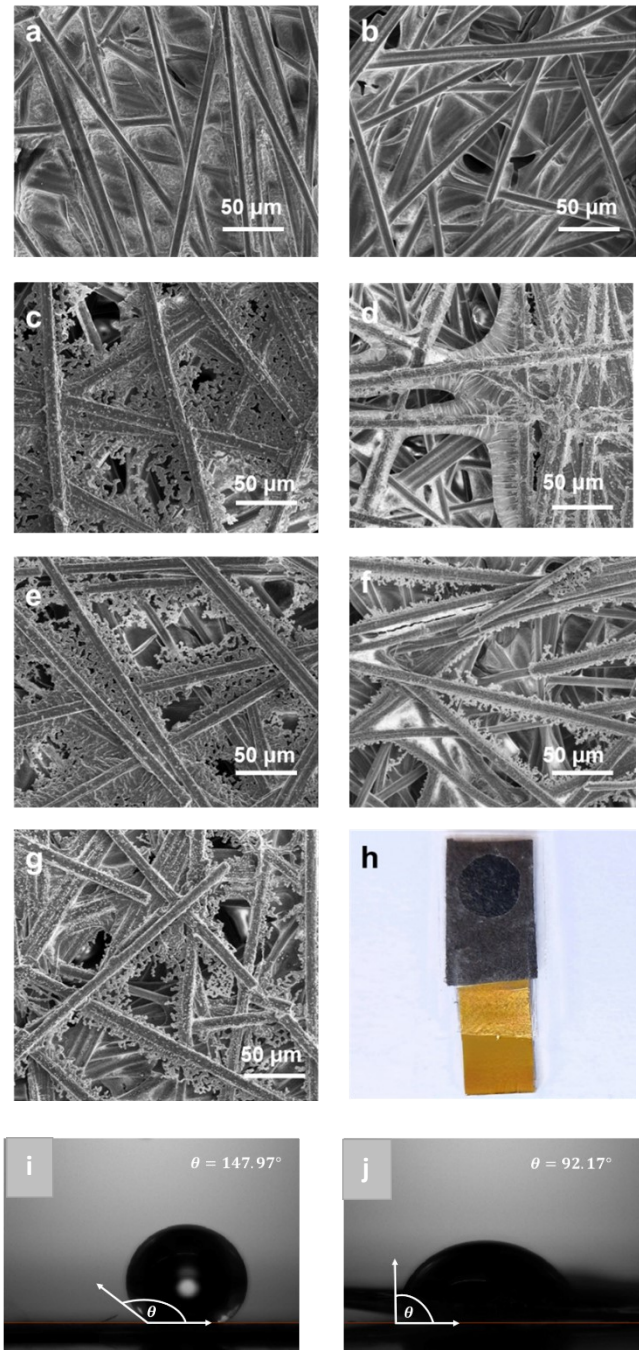

Figure S9. SEM images of (a and b) non-modified carbon paper or carbon paper decorated with (c and d) MIP, (e and f) NIP and, (g) pristine PPy, (a, c, e, g) before or (b, d, f) after 60 minutes of extraction in 0.1 M carbonate buffer of pH = 9.1. (h) Optical camera image of MIP film-coated carbon electrode. Water contact angles measured for (i) pristine carbon paper and (j) electrodeposited MIP film on the carbon paper.

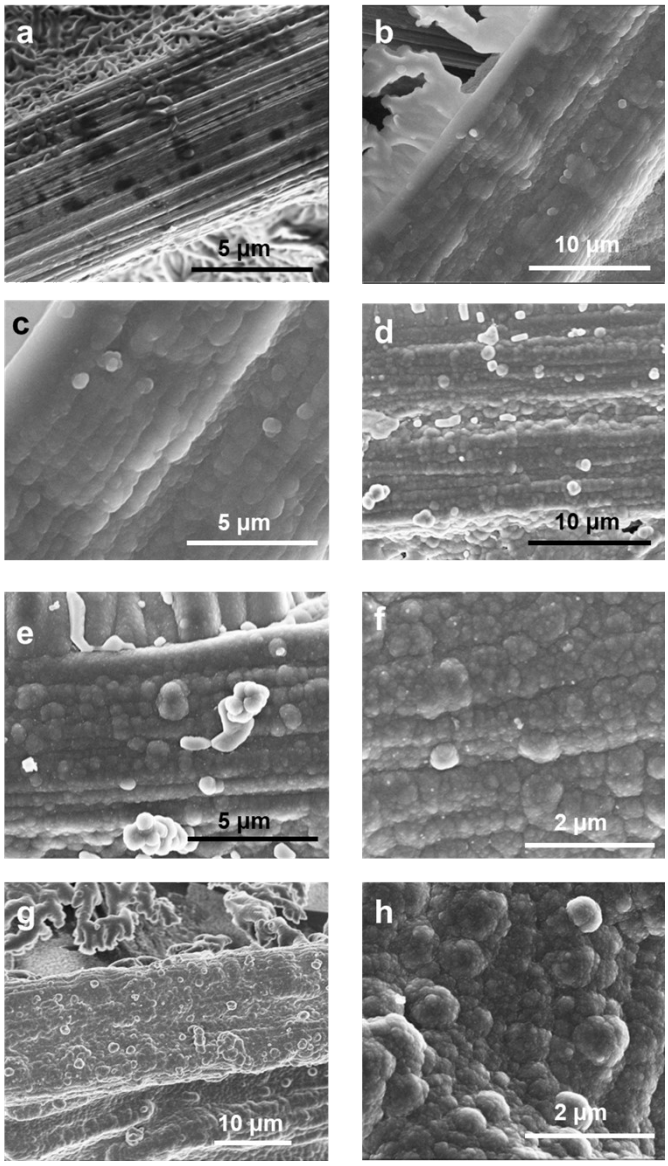

Figure S10. SEM images covering wider areas of (a) non-modified carbon paper or carbon paper decorated with (b–f) MIP and (g and h) NIP, (a, b, c, g, and h) without or (d, e, and f) after 60 minutes of extraction in 0.1 M carbonate buffer of pH = 9.1.

S5. Spectroscopic characterization of the MIP and NIP films

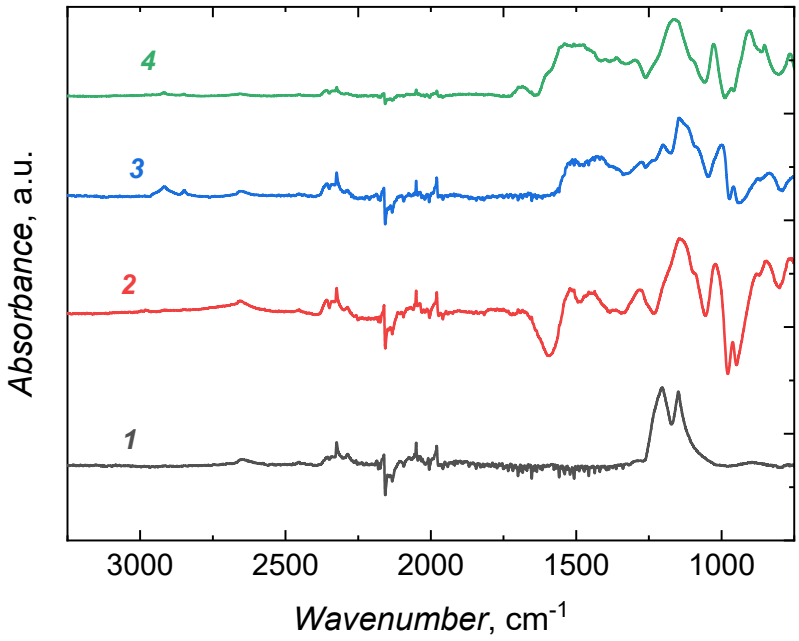

Figure S11. ATR-IR spectrum of (1) carbon paper, (2) bare polypyrrole film, (3) NIP, and (4) MIP film.

S6. XPS analysis of the MIP and NIP-coated electrodes

Table S1. Quantitative XPS atomic content of the fabricated electrodes.

Sample name	Atomic content of element, [%]							
	C	O	N	F	Si	S	Na	Cl
Pristine carbon paper	50.08	2.76	0.25	45.66	1.28	–	–	–
PPy-coated carbon paper	72.7	10.05	3.96	10.05	0.95	0.45	0.76	1.88
MIP-coated carbon paper before extraction	60.16	5.08	4.08	28.39	1.33	–	–	0.95
MIP-coated carbon paper after extraction	70.97	11	7.02	8.62	–	1.04	1.36	–
NIP-coated carbon paper before extraction	68.78	9.37	4.86	15.19	0.99	0.2	–	0.6

The fluorine content in samples was detected due to the fluorinated carbon paper used to deposit MIP and NIP films. The silicon content results from the trace amounts of silicon carbide added during the production of carbon paper [1].

Sulfur in the form of SO_4^{2-} may be a contaminant of KCl and sodium carbonate and bicarbonate used to prepare the buffer. Difficulties in washing out these ions may suggest the doping of polypyrrole with sulfates, which was also previously reported[2]. The trace content of

sodium in the sample after the electrodeposition of PPy was a minor impurity of KCl, acting as the supporting electrolyte during the electrodeposition.

Chlorine undoubtedly comes from the supporting electrolyte KCl used during polymer electrodeposition. Chloride anions are doped during polymerization to maintain the electroneutrality of the system, compensating for the positively charged cation radicals of polypyrrole.

S7. Testing of the electrode robustness

The MIP-coated electrode was prepared according to the protocol described in the Experimental Section. Forty CV cycles were recorded to stabilize the layer (−0.5 to 0.1 V vs. Ag quasi-reference electrode, 50 mV s^{-1}), and three DPV measurements (−0.5 to 0.1 V vs. Ag quasi-reference electrode, 10 mV s^{-1}). Subsequently, the MIP-coated carbon paper electrode was removed from the solution and bent 10 times by about 45°. Then, CV (10 cycles), and DPV (5 measurements) were re-recorded. Analogous measurements were also carried out after bending 30 and 100 times. The last CV cycles of the measurements are shown in Figure S11a. Similarly, the exact measurement was taken in a solution containing 9.9 nM **MTZ (**Figure S11b).

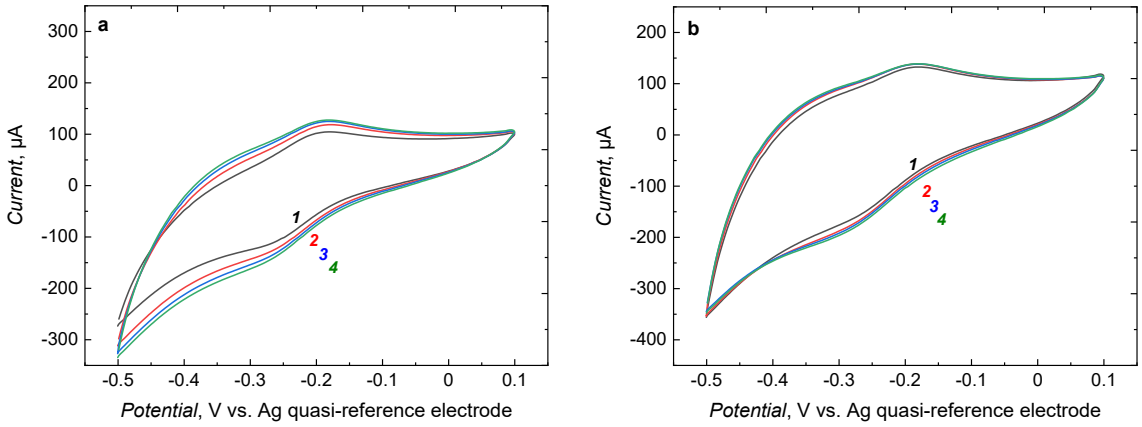

Figure S12. CV curves recorded in the presence of 1 mM $Ru(NH_3)_6Cl_3$ solution in 0.1 M $KCl_{(aq)}$ over (a) pristine carbon paper electrode and (b) in the presence of 9.9 nM of **MTZ** on the MIP film-coated electrode after bending by about 45°: (*1*) 0, (*2*) 10, (*3*) 30, and (*4*) 100 times.

S8. Testing Py to Py-COOH composition for MIP and NIP synthesis

Finding the proper cross-linker to functional monomer ratio is almost as important for successful MIP synthesis as choosing proper functional monomers. The cross-linking monomer, namely Py, builds up the polymer matrix and thus ensures proper geometry of imprinted molecular cavities. This geometry should remain unaffected after template

extraction. Too high concentration of Py would result in a low population of imprinted cavities in the polymer matrix and thus in low sensitivity of the devised sensor. If Py concentration is too low, MIP would not be crosslinked enough, and imprinted cavities would collapse after **MTZ** template extraction. Therefore, MIP and NIP films were prepared with two times higher concentrations of **Py-COOH** and **MTZ**. Responses to **MTZ** was almost indistinguishable on MIP and NIP-coated electrodes (Figures S13 and S14). Only at concentrations above 100 nM of **MTZ** MIP coated electrode started to show response. Therefore, previously tested functional and crosslinking monomer composition (100:1 ratio) for MIP preparation was decided to be the optimal one and used in further studies.

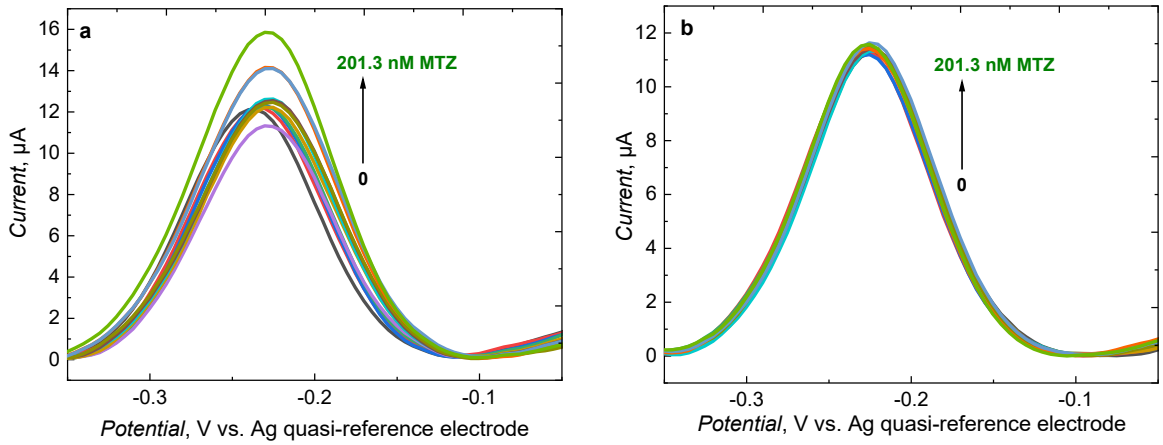

Figure S13. DPV curves recorded on the extracted (a) MIP or (b) NIP film-coated carbon paper electrodes obtained by polymerization of 0.1 M Py, 2 mM **Py-COOH** (50:1 ratio), and (a) 1 mM **MTZ** or (b) without **MTZ** in 1.0 M KCl/H_2O.

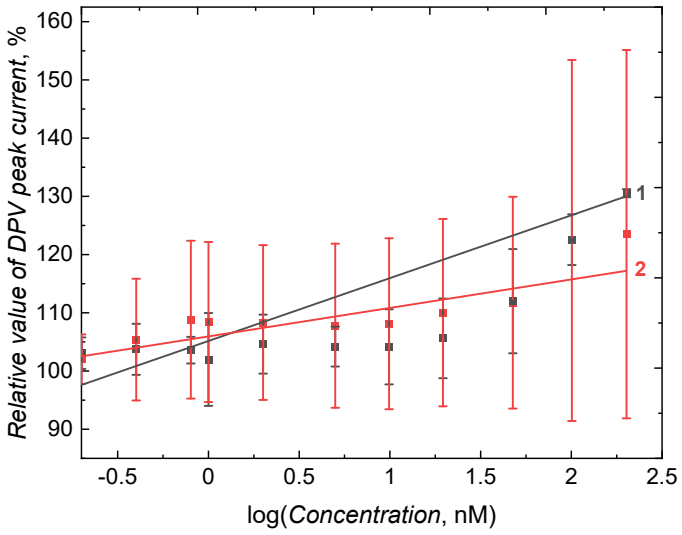

Figure S14. Calibration curves constructed for DPV peak current recorded on carbon paper electrodes coated with (*1*) MIP and (*2*) NIP. MIP film was deposited from a solution containing Py:**Py-COOH**:**MTZ** in a 50:1:0.5 ratio.

S9. Reproducibility of the MIP-coated electrode fabrication procedure

Five independent electrodes were prepared and coated with MIP films following the same procedure. Then, a change of the DPV signal after 0.2 nM **MTZ** injection was tested (Figure S15). Each DPV was measured in triplicate. The standard deviation of DPV response between five different electrodes was 1.26% and for five measurements performed on each of these electrodes was between 0.75% and 3.1%, depending on the electrode, proving excellent reproducibility of the MIP-coated electrode fabrication procedure.

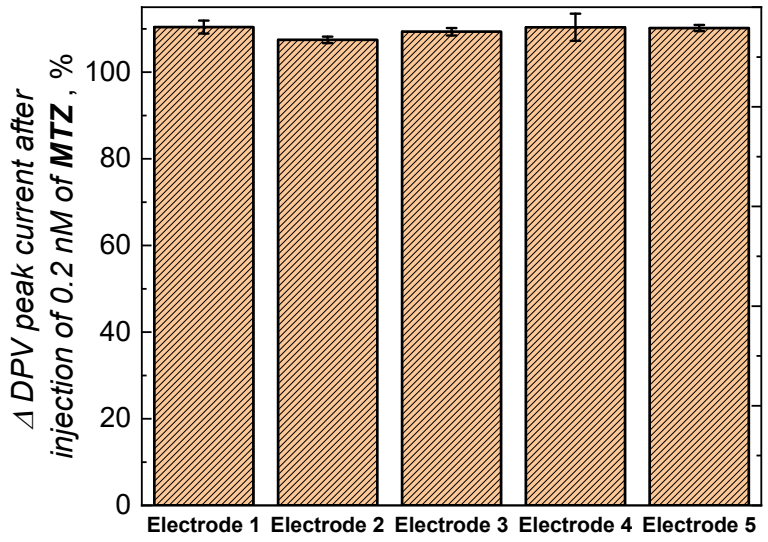

Figure S15. DPV response to injection of 0.2 nM **MTZ** recorded for five individual electrodes in the presence of 1 mM $Ru(NH_3)_6Cl_3$ in 0.1 M $KCl_{(aq)}$.

S10. Stability of the MIP-coated electrodes

The shelf-life of MIP-coated electrodes was evaluated. Change of the DPV signal after 0.2 nM **MTZ** injection for electrodes stored for 0, 3, and 7 days at 4 °C was tested (Figure S16). Each DPV was measured three times. After three days of storage, no change of electrode response to **MTZ** was observed. However, after storing for one week, the electrode response became higher and more irreproducible. Presumably, because of partial damage in the sealing of the electrode. Therefore, electrodes were used within three days after fabrication in all experiments.

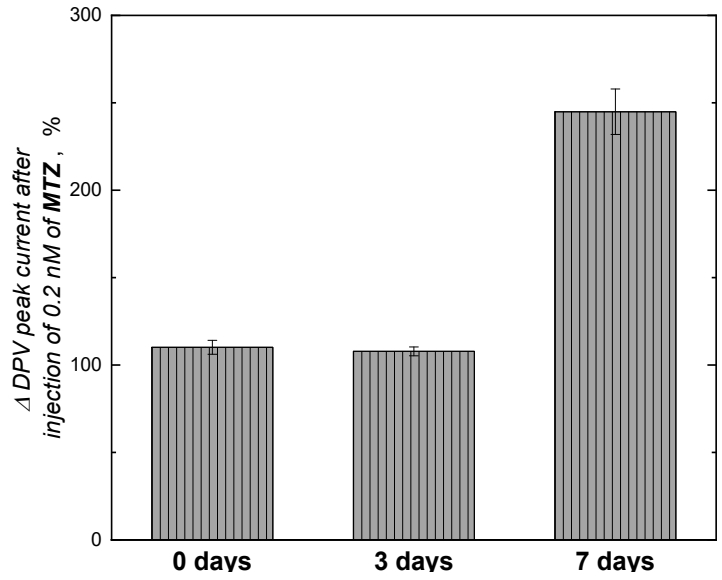

Figure S16. DPV response to injection of 0.2 nM **MTZ** recorded for three individual electrodes in the presence of 1 mM $Ru(NH_3)_6Cl_3$ solution in 0.1 M $KCl_{(aq)}$ after storing them on air.

S11. Studies on the electrochemical properties of a carbon paper substrate

The obvious choice of hexaammineruthenium chloride as the main redox probe was based on it charge which is opposite to the negatively charged polymer (due to the carboxyl group presence). Moreover, this redox probe is known to follow the outer-sphere electron transfer mechanism, in which no specific interactions with the electrode are expected.[3] In contrast, the redox probes described by inner-sphere electron transfer, for instance potassium hexacyanoferrates(II) and (III), interaction with electrode is anticipated.

Herein, MIP layers were deposited on carbon paper, due to that, we obtained a porous and surface developed layer. It is expected that the adsorption of species on the MIP surface must be limited only to the target analyte in order to obtain the desired sensor selectivity. This condition perfectly suited for application of outer-sphere redox probe.

We have recorded a series of cyclic voltammograms on the MIP film after extraction of **MTZ** in the equimolar composition of 1 mM $K_3Fe(CN)_6/K_4Fe(CN)_6$ or in 1 mM $Ru(NH_3)_6Cl_3$ (supporting electrolyte: aqueous solution of 0.1 M KCl in both cases) for a series of scan rates of 5–500 mVs^{-1} (Figure S17 a–b).

In both cases, presence of a pair of redox peaks originating from oxidation and reduction of the redox probe is observed, with higher current values obtained for the redox pair $K_3/K_4Fe(CN)_6$. Higher current is associated with high diffusion coefficient of hexacyanoferrates in comparison to hexaammineruthenium ions.[4, 5]

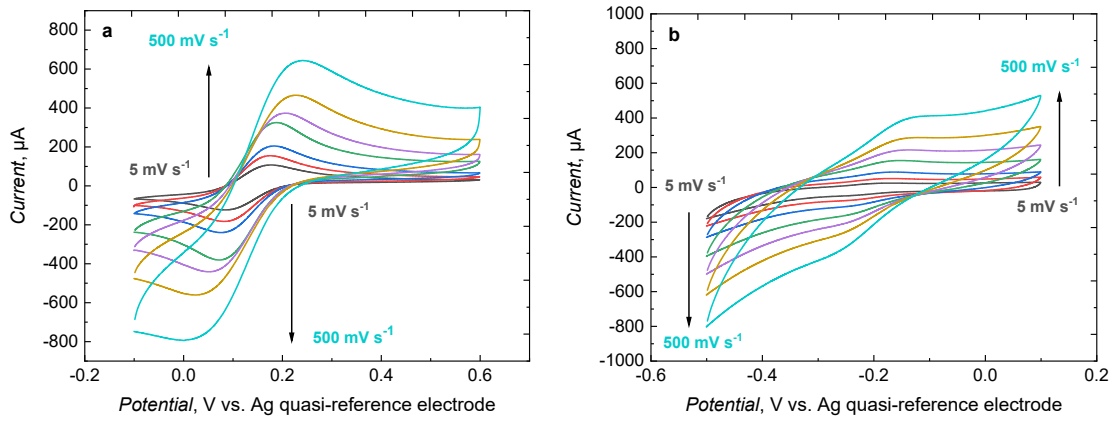

Figure S17. Cyclic voltammograms recorded on MIP film electropolymerized on carbon paper, after analyte extraction in solution containing (a) 1 mM $K_3/K_4Fe(CN)_6$ and (b) 1 mM $Ru(NH_3)_6Cl_3$ in 0.1 M KCl with 5–500 mV s^{-1} scan rates.

The dependence of the peak current on the square root of the scan rate in both cases is linear in the range of 5–50 mV s^{-1} (Figure S18 a–b), being in line with Randles-Sevčik equation.

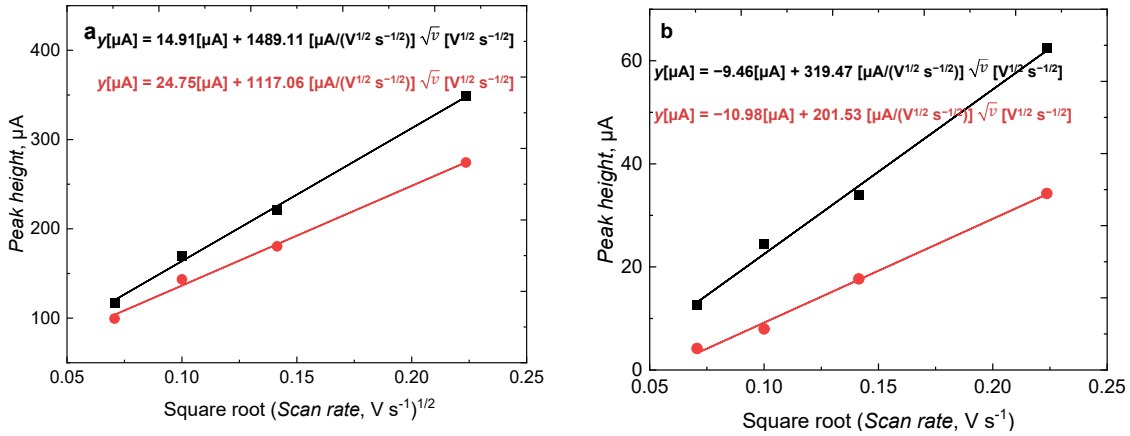

Figure S18. Anodic and cathodic peak current heights (black and red square, respectively, with fitted linear regression lines) as a function of the square root of scan rates $\sqrt{v}$ (5–50 mV s^{-1}) obtained from analysis of the CV curves in Figure S17 for (a) 1 mM $K_3/K_4Fe(CN)_6$ and (b) 1 mM $Ru(NH_3)_6Cl_3$.

Despite the higher slopes of the curves in Figure S18a compared to Figure S18b, the values of the separation of the oxidation and reduction peaks for both redox probes are worth considering, as they directly describe the rate of the electron transfer process. The redox pair, $Fe(CN)_6^{3-/4-}$, as a representative of the inner-sphere electron transfer (ISET) mechanism, is characterized by higher peak-to-peak separation values than the redox pair $Ru(NH_3)_6^{2+/3+}$, in which the electron transfer occurs according to the outer-sphere (OSET) mechanism (Figure

S19). The greater separation of the cathodic and anodic peaks results from the slower electron transfer process, since the ISET mechanism is explained by the bridging effect, i.e., the formation of a temporary oxidant and reductant complex adsorbed on the electrode surface, constituting an intermediate stage in the electron transfer, limiting its rate.

During electron transfer within the ruthenium redox probe, according to the OSET mechanism, no intermediate complex is formed and no adsorption of redox probe ions occurs. Hence the smaller separation of peaks is observed.[3] Presumably the absorption of $Fe(CN)_6^{3-}$ and $Fe(CN)_6^{4-}$ on the MIP-coated electrode surface made it difficult to obtain a stable redox signal during CV measurements. Recorded peaks decreased with each subsequent cycle without adding any analyte. Opposite to this, in the case $Ru(NH_3)_6^{2+/3+}$, we did not observe this phenomenon, the height of the peak was constant during multiple cycling, therefore this probe was used in the study.

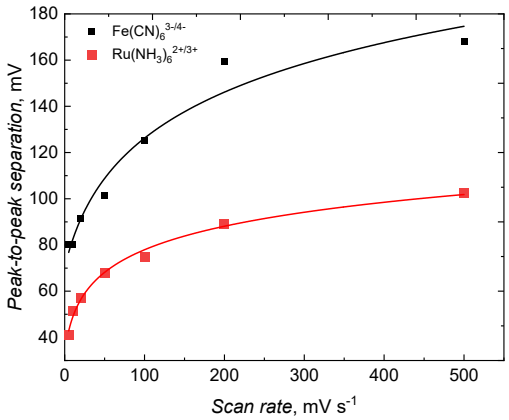

Figure S19. Comparison of peak-to-peak separation in the voltammograms calculated from Figure S17 for $Fe(CN)_6^{3-/4-}$ (black squares) and $Ru(NH_3)_6^{2+/3+}$ (red squares).

The preliminary results obtained in the presence of 1 mM potassium hexacyanoferrates(II) and (III) did not provide satisfactory results due to the competition of $Fe(CN)_6^{3-}$ and $Fe(CN)_6^{4-}$ ions with **MTZ** molecules in interaction with the porous electrode further justify the choice. Adsorption of redox probe ions prevented selective adsorption of analyte molecules in the molecular cavities of MIP. That is why, we obtained irreproducible results.

Table S2. MIP-based sensors for **MTZ** determination.

No.	Transduction method	Details of MIP fabrication	Dynamic concentration range	LOD	IF	Sensitivity	Selectivity factors	Stability	Reference
1	Fluorescence	Imprinted polydopamine shell was chemically synthesized over MIL-53(Fe) MOF NPs core	1–200 μM	53.4 nM	–	$0.201\log(c_{MTZ}$ [μmol L^{-1}])	Response ratio for intereferents up to 0.02 (SF = 50) compared to **MTZ**	–	6
2	Electro reduction observed with DPV	Poly(anilinomethyltriethoxy silane) condensed with 3-aminopropyltriethoxysilane tetraethylorthosilicate	0.4–200 μM	91 nM	–	$0.0212c_{MTZ}$ [μmol L^{-1}]	–	Up to 30 days	7
3	Fluorescence	Magnetic molecularly imprinted polymer-based fluorescent probe	0–5 μM	4.9 nM	2.9	1.20744×10^{-4} c_{MTZ} [μmol L^{-1}]	–	–	8
4	Electrocatalytic reduction observed with DPV	Poly(copper–melamine complex) imprinting matrix	0.5–1000 μM	0.12 μM	4	$0.0204c_{MTZ}$ [μmol L^{-1}]	A response to interferents below 5% compared to **MTZ**	12% decay after two months storage	9
5	Potentiometry	Imprinted co-polymer of 1-vinyl-2-pyrrolidine and ethylene glycol dimethacrylate (EGDMA) particles synthesized via precipitation polymerization	10 nM – 1 mM	7 nM	–	61.5 ± 0.5, mV/decade	–	A relatively long lifespan (≥4 months)	10
6	CV in presence of $K_{3/4}[Fe(CN)_6]$ redox probe	*o*-Phenylenediamine MIP film electropolymerized over 3D nanoporous nickel	60–400 fM and 0.4–4 pM	20 fM	–	–	–	A response of 96.6% of the initial current after 30 days of storage	11
7	Electroreduction of **MTZ** observed with DPV	Imprinted co-polymer of methacrylic acid and EGDMA	56.4 ng/mL – 2.6 μg/mL and 2.6 μg/mL –	35.9 ng/mL	–	$4812.0c_{MTZ}$ [mg L^{-1}] and 184.12	Signal change below 5% in	–	12

		was grounded and mixed with carbon paste	76.9 µg/mL			c_{MTZ} [mg L^{-1}], respectively	the presence of over 100-fold excess concentration of intereferents		
8	Electroreduction of **MTZ** observed with DPV	Imprinted *o*-phenylenediamine film deposited with electropolymerization	1–10 nM	0.33 nM	–	0.1081 c_{MTZ} [nmol L^{-1}]	–	7.8% signal decrease after 30 days of storage	[13]
	CV in presence of $K_{3/4}[Fe(CN)_6]$ redox probe		2–100 nM (semilog scale)	0.67 nM	–	0.0931 ln(c_{MTZ} [mol L^{-1}])	–	4.1% signal decrease after 30 days of storage	
9	Electroreduction of **MTZ** observed with DPV	Imprinted polypyrrole electropolymerized over electrode surface decorated with 2D Sn_3O_4 flakes	25 nM – 2.5 µM	3.2 nM	~10	2.14 c_{MTZ} [µmol L^{-1}]	–	8.0% signal decrease afer storage for 3 weeks at room temperature	[14]
10	Electroreduction of **MTZ** observed with DPV	(Imprinted silica)/(graphene quantum dots) NPs were drop-cast on graphene nanoplatelets decorated electrode	5–750 nM and 0.75–10 µM	0.52 nM	–	23.292 c_{MTZ} [µmol L^{-1}] and 2.9863 c_{MTZ} [µmol L^{-1}], respectively	Up to 500 units (*w*/*w*) of Na^+, K^+, and glucose in the presence of 0.5 µmol L^{-1} **MTZ**	–	[15]
11	Electroreduction of **MTZ** observed with DPV	Imprinted aniline electropolymerized over electrode surface decorated with $CuCo_2O_4$ NPs and nitrogen-doped carbon nanotubes	5–100 nM and 0.1–100 µM	0.48 nM	~1.8	4.1901 c_{MTZ} [µmol L^{-1}] and 0.3462 c_{MTZ} [µmol L^{-1}], respectively	Peak current change value ≤ 5% in the presence of interferents	96% of the initial current response after two weeks of storage	[16]
12	DPV in the presence of $Ru(NH_3)_6Cl_3$ redox probe	Imprinted co-polymer of 3-(1*H*-pyrrol-1-yl)propanoic acid and pyrrole electropolymerized on the carbon paper electrode	0.2–200 nM	0.4 nM	38	17.82/log(n mol L^{-1})	26.1 for glucose	12–14% decay after a week storage	This work

Table S3. Electrochemical sensors for **MTZ** determination.

No.	Transduction method	Electrode modification	Dynamic concentration range	LOD	Selectivity	Sensitivity	Stability	Real sample measured	Reference
1	Amperometry	Mn(III) complex of 5,10,15,20-tetrakis [2-(2,3,4,6-tetraacetyl-*β*-D-glucopyranosyl)-1-*O*-phenyl]porphyrin included in graphite-epoxy resin	2.9 mM – 58 nM	58 nM	Presence of hexacyanoferrate(II), Fe^{3+}, Cu^{2+}, ascorbic acid, albendazole, NO_3^- and *o*-aminophenol in 0.5 mM caused ≤ 3% change in the signal	25.2 ± 1.3 µA/decade	Disposable, can stored in refrigenerator for 2 months	-	17
2	Potentiometry	PVC membrane with 2,6-(*p*-*N*,*N*-dimethylaminophenyl)-4-phenylthiopyrylium perchlorate	0.1 M – 10 µM	8 µM	For I^-, SCN^-, and L-histidine selectivity coefficients were equal to 2.6×10^{-2}, 3.1×10^{-3}, 4.1×10^{-3}, for other interfering ions these factors were in range of 10^{-5}	33.3 ± 0.1 mV/decade	-	Synthetic serum sample, pharmaceutical preparations (tablet, gel and injection)	18
3	Linear sweep stripping voltammetry	Electrodeposited copper-poly(cysteine) film	0.5 – 400 µM	370 nM	1000-fold concentration of Al^{3+}, Ca^{2+}, Mg^{2+}, Zn^{2+}, Na^+, SO_4^{2-}, F^- and Cl^-, 10-fold concentration of cysteine, ascorbic acid, oxalic acid, fructose, caffeine and glucose do not affect the signals of metronidazole (signal change below 5%)	98 mA/M	The current response decayed by 9% after two months storage	Injection solution	19
4	Square wave voltammetry	Boron-doped diamond electrode	0.2 – 4.2 µM	65 nM	-	25.5 A/(M×cm^2)	-	Injection solution, human urine	20
5	DPV	Electropolymerized of *α*-cyclodextrin	0.5 – 103 µM	280 ± 20 nM	Signal change of 2.68% in presence of paracetamol in a 60-fold concentration	119 mA/M	The peak current intensity decreased 6% after 1 week of storage	Injection solution	21

6	DPV	Pt nanospheres/polyfurfural film modified electrode	2.5 to 500 μM	50 nM	Presence of NO_3^-, Cl^-, PO_4^{3-}, SO_4^{2-}, F^-, CO_3^{2-}, Na^+, Ca^{2+}, K^+, Mg^{2+}, Zn^{2+}, NH_4^+, K^+ and Ac^- in 1000-fold concentrations; ascorbic acid, oxalic acid, dopamine, cystine, alanine, glucose, citric and tartaric acid in 100-fold concentrations; imidazole, benzimidazole, 2-methylimidazole, nifedipine, nitrendipine and nitrophenol in 10-fold concentrations, caused signal change below 5%	-26.5 mA/M	1 month of storing in a refrigerator	Human serum	22
7	DPV	Multi-walled carbon nanotubes and chitosan-nickel complex modified electrode	0.1 – 150 μM	25 nM	Presence 300-fold of glucose, lactose, sucrose, urea, Cu^{2+}, Fe^{2+}, Co^{2+}; 150-fold of cholesterol, thiamine hydrochloride, starch, cysteine, oxalic acid, fructose, caffeine; 50-fold of ascorbic acid, uric acid, aminoacetic acid caused signal change below 5%	695 mA/M	Retained 90% of its initial value after the storage of a week in a refrigerator	Tablet, human serum, urine	23
8	Linear sweep voltammetry	Biomass-derived N, S, P-triple-doped porous carbon	0.1 – 350 μM	13 nM	Presence of chloramphenicol, dopamine, nitro phenol, uric acid, glucose, ascorbic acid, thiamphenicol, Vitamin E, and florfenicol caused signal change below 5%	298.5 mA/M	Signal decrease of 5% after two weeks of storing in the fridge	Tablet, injection solution, milk	24
9	DPV	Carbon paste electrode modified with Al_2O_3 microparticles that are hydrothermally formed on the graphite carbon sheet	0.5 μM – 1 mM	256 nM	Moderate selectivity. Presence of K^+, Cu^{2+}, Fe^{2+}, Mg^{2+}, Zn^{2+}, SO_4^{2-}, Cl^-, Na^+, Ca^{2+}, and CO_3^{2-} caused drop of the signal by about 10%	-5.5 A/M	Retained 96% of its initial response after 20 days	Urine, tap water and river water	25
10	Adsorptive stripping square wave voltammetry	AgNPs functionalized CuMOF/PPy–rGO nanocomposite decorated electrode	80 nM – 160 μM	24 nM	200-fold excess of Cu^{2+}, Mg^{2+}, K^+, Fe^{2+}, SO_4^{2-}, Na^+, and Cl^-, 80-fold excess of urea, sucrose, and glucose, 50-fold excess of cysteine, 20-fold excess of citric acid,	-70 mA/M	-	Tablet and human urine	26

					uric acid, and ascorbic acid, and 10-fold of tartaric acid did not affect the detection of **MTZ**				
11	DPV	Composite of MnOOH nanorods and expanded graphite	70 nM –3 0 µM	17 nM	No influence was found for the quantification of 5 µM **MTZ** in 0.1 M PBS containing inorganic interfering substances (Na^+, K^+, Ca^{2+}, Zn^{2+}, Al^{3+} and Mg^{2+}), urea and glucose at 0.25 mM, lactose, ascorbic acid and amoxicillin at 100 µM or azathioprine, niclosamide, chloram phenicol, *p*-nitrophenol, *o*-nitrophenol at 1 µM	223.5 mA/M	-	Tablet, capsule, lake water	[27]
12	Amperometry	Fe_2O_3 nanoparticle-graphene oxide nanocomposites modified glassy carbon electrode	1 µM – 1.6 mM	55 nM	Caffeine, cystine, cellulose, glucose, chloramphenicol, dopamine, nitrophenol, ascorbic acid, thiamphenicol, oxalic acid, 4-nitrobenzoic acid, uric acid, orinidazole, 4-nitroaniline, florfenicol, 4-nitrophenol, KCl, $NaNO_3$, $CaCl_2$ and $MgSO_4$ in five times higher concentration caused signal chnge at level of 2-10% of response to **MTZ**	22 mA/M	-	Urine	[28]
13	DPV	Gold nanoparticle modified carbon nanofiber	100 nM – 2 mM	24 nM	Ascorbic acid, tetracycline and L-phenylalanine were added with 10 times higher concentration; and of Fe^{3+}, Zn^{2+}, Na^+, K^+ and Sn^{4+} is 30 times higher, the signal change was lawer than 5% response to **MTZ**	10 mA/M	-	Tap water	[29]
14	DPV	*N*,*S*-Doped carbon dots and amine-grafted graphene oxide	50 nM – 100 µM	10 nM	Presence of $CuCl_2$, $Fe(NO_3)_3$, $CaCl_2$, NaCl, $MgSO_4$, vitamin C, adrenaline, tryptofan, folic acid, H_2O_2, glucose, and L-cystein cayse current response	554.5 mA/M	-	Plasma sample	[30]

					equal to 0.5-2.5% of response to **MTZ**				
15	DPV	Electrode decorated with composite MoS_2 and graphitic carbon nitride	2 – 125 μM	99 nM	4-Nitroimidazole, ronidazole, 1,2-dimethylimidazole, L-cysteine, dimetridazole, α-phenylethylamine, Ca^{2+}, Cl^-, hydrazine, chlorophenol, nitrophenol, hydrogen peroxide, uric acid, urea, and glucose presence caused signal change below 5%	2.85 A/(M×cm^2)	Sensor retained >80 % of its initial current response after 28 days	-	[31]
16	DPV	Flower-like cobalt anchored on reduced graphene oxide nanocomposite	25 pM – 500 nM	15 pM	Presence of NH_4F, $Mg(NO_3)_2$, Na_2SO_4, K_3PO_4, $CaCl_2$, $Zn(Ac)_2$, K_2CO_3, in concentration 5000 times higher, and tartaric acid, citric acid, glucose, oxalic acid, ascorbic acid, dopamine, uric acid, cysteine, nifedipine, nitrendipine, nitrofurazone, and nitrophenol in concentration 500 higer than **MTZ** caused signal chnge equal to 1-6%	66.1 A/M	-	Human serum	[32]
17	Square wave voltammetry	Thermally annealed gold-silver nanoporous alloy integrated with reduced graphene oxide and poly(glycine) at the surface of a glassy carbon electrode	2.0 pM – 410 μM	31.2 fM	In the presence of a 200-fold excess concentration of antibiotics (cephalexin, erythromycin, azithromycin, tinidazole, ampicillin, amoxicillin, cloxacillin, chloramphenicol, and ciprofloxacin), a 600-fold excess of organic molecules (dopamine, glucose, ascorbic acid, fructose, folic acid, urea, sucrose, uric acid, and lactose), and an 850-fold excess of inorganic substances (Cu^{2+}, Fe^{3+}, HCO_3^-, NO_3^-, Ca^{2+}, Mg^{2+}, SO_4^{2-} and CO_3^{2-}) relative percentage error of the current response remained below 5%	980 mA/M	Response of the sensor decreased by 4.4% after the eighth week	Milk powder, pork and chicken meat	[33]

18	Amperometry	Co_9S_8@MoS_2 core–shell nanoparticles decorated with reduced graphene oxide	0.5 – 35.0 μM	380 nM	Sensor didn't respond to the uric acid, oxalic acid, malic acid, glucose, ascorbic acid, and acetaminophen, as well as Cl^-, NO_3^-, Cu^{2+}, Fe^{2+}, Fe^{3+}, Na^+, and K^+ presence	-1.2 A/M	Peak current decreased by 4.8% after 7 days	Blood plasma and tablet samples	[34]
19	DPV	Ni,Ti-MOF	0.1 – 200 μM	30 nM	Sensor shows similr response to oxazepam	-55.7 μA/decade	Signal decay by 5.45% after one month of storage	Human blood plasma	[35]
20	DPV	g-C_3N_4/MnO_2/ZnO modified electrode	2 – 250 μM	210 nM	Presence of ornidazole, tetracycline, norfloxacin, chloramphenicol, glucose and fructose caused signal change below 5%	-160 mA/M	After a 30-day storage 91.5% response retained	Honey	[36]
21	DPV	Carbon dots stabilized Ag nanoparticles and gallic acid stabilized Cu_2O nanoparticles	10 – 110 μM	710 nM	Presence of 100-fold concentration of amoxicillin, ciprofloxacin, chloramphenicol, disclofenic sodium, dopamine, ascorbic acid, NO_3^- and Ca^{2+} did not produce any notable change in the reduction current of **MTZ**	1.5 A/(M×cm^2)	Reduction peak current decay by 9.2% for the **MTZ** after four weeks	Milk	[37]
22	DPV	(Pr, Gd, and Sm) VO_4	-	1.5 nM	Electrode shows similar response to furazolidone	-	-	Bovine serum, human urine, river water	[38]
23	DPV in the presence of $Ru(NH_3)_6Cl_3$ redox probe	Imprinted co-polymer of 3-(1*H*-pyrrol-1-yl)propanoic acid and pyrrole electropolymerized on the carbon paper electrode	0.2–200 nM	0.4 nM	26 times lower response to glucose, neglidible response to glyphosate, creatinine, L-ascorbic acid, penicillin G, and vancomycin	17.82 %/decade	12–14% decay after a week storage	Honey	This work

References

1. J. Chen, P. Xiao and X. Xiong, *Mater. Des.*, 2015, **84**, 285-290.

2. A. Kisiel, D. Korol, A. Michalska and K. Maksymiuk, *Electrochim. Acta*, 2021, **390**, 138787.

3. N. Kurapati, P. Pathirathna, C. J. Ziegler and S. Amemiya, *ChemElectroChem*, 2019, **6**, 5651-5660.

4. A. J. Arvía, J. C. Bazán and J. S. W. Carrozza, *Electrochim. Acta*, 1968, **13**, 81-90.

5. Y. Wang, J. G. Limon-Petersen and R. G. Compton, *J. Electroanal. Chem.*, 2011, **652**, 13-17.

6. Z. Zhang, Y. Liu, P. Huang, F.-Y. Wu and L. Ma, *Talanta*, 2021, **232**, 122411.

7. N. Xiao, JianDeng, J. Cheng, S. Ju, H. Zhao, J. Xie, D. Qian and J. He, *Biosens. Bioelectron.*, 2016, **81**, 54–60.

8. N.-D. Tan, C. Lan, J.-H. Yin, L. Meng and N. Xu, *Bull. Korean Chem. Soc.*, 2020, **41**, 60–65.

9. Y. Gu, X. Yan, C. Li, B. Zheng, Y. Li, W. Liu, Z. Zhang and M. Yang, *Biosens. Bioelectron.*, 2016, **77**, 393–399.

10. M. El-Beshlawy and H. Arida, *Micromachines*, 2022, **13**, 2107.

11. Y. Li, Y. Liu, Y. Yang, F. Yu, J. Liu, H. Song, J. Liu, H. Tang, B.-C. Ye and Z. Sun, *ACS Applied Materials & Interfaces*, 2015, **7**, 15474-15480.

12. M. B. Gholivand and M. Torkashvand, *Talanta*, 2011, **84**, 905-912.

13. J. Liu, H. Tang, B. Zhang, X. Deng, F. Zhao, P. Zuo, B.-C. Ye and Y. Li, *Anal. Bioanal. Chem.*, 2016, **408**, 4287-4295.

14. J. Wang, W. Du, X. Huang, J. Hu, W. Xia, D. Jin, Y. Shu, Q. Xu and X. Hu, *Analytical Methods*, 2018, **10**, 4985-4994.

15. A. A. Ensafi, P. Nasr-Esfahani and B. Rezaei, *Sens. Actuators, B*, 2018, **270**, 192-199.

16. Y. Wang, L. Yao, X. Liu, J. Cheng, W. Liu, T. Liu, M. Sun, L. Zhao, F. Ding, Z. Lu, P. Zou, X. Wang, Q. Zhao and H. Rao, *Biosens. Bioelectron.*, 2019, **142**, 111483.

17. F.-C. Gong, X.-B. Zhang, C.-C. Guo, G.-L. Shen and R.-Q. Yu, *Sensors*, 2003, **3**, 91-100.

18. M. R. Ganjali, P. Norouzi, F. Faridbod and H. Pirelahi, *J. Chin. Chem. Soc.*, 2013, **54**, 55-61.

19. Y. Gu, X. Yan, W. Liu, C. Li, R. Chen, L. Tang, Z. Zhang and M. Yang, *Electrochim. Acta*, 2015, **152**, 108-116.

20. H. B. Ammar, M. B. Brahim, R. Abdelhédi and Y. Samet, *Mater. Sci. Eng. C*, 2016, **59**, 604-610.

21. A. Hernández-Jiménez, G. Roa-Morales, H. Reyes-Pérez, P. Balderas-Hernández, C. E. Barrera-Díaz and M. Bernabé-Pineda, *Electroanalysis*, 2015, **28**, 704-710.

22. J. Huang, X. Shen, R. Wang, Q. Zeng and L. Wang, *RSC Advances*, 2017, **7**, 535-542.

23. A. Mao, H. Li, L. Yu and X. Hu, *J. Electroanal. Chem.*, 2017, **799**, 257-262.

24. N. Yalikun, X. Mamat, Y. Li, X. Hu, P. Wang and G. Hu, *J. Electrochem. Soc.*, 2019, **166**, B1131-B1137.

25. J. Zoubir, C. Radaa, A. Idlahcen, I. Bakas and A. Assabbane, *Mater. Sci. Energy Technol.*, 2021, **4**, 296-306.

26. H. Saedi, M. R. Fat'hi and B. Zargar, *J. Chin. Chem. Soc.*, 2021, **68**, 1954-1964.

27. X. Hu, Y. Zhang, T. Zeng, Q. Wan, K. Wu and N. Yang, *Diam. Relat. Mater.*, 2022, **128**, 109303.

28. Z. Liu, Z. Wang and Y. Xu, *Int. J. Electrochem. Sci.*, 2022, **17**, 220731.

29. L. Zhang, M. Yin, J. Qiu, T. Qiu, Y. Chen, S. Qi, X. Wei, X. Tian and D. Xu, *Biosens. Bioelectron. X*, 2022, **10**, 100102.

30. M. Saleh-Mohammadnia, M. Ghalkhani, H. Roghani-Mamaqani, S. Hemmati and H. Mardani, *IEEE Sensors Journal*, 2023, **23**, 18986-18993.

31. K. Ahmad, W. Raza, A. Alsulmi and H. Kim, *Diam. Relat. Mater.*, 2023, **138**, 110178.

32. J. Huang, Z. Qiu, J. Lin, J. Lin, F. Zhu, G. Lai and Y. Li, *Microchem. J.*, 2023, **188**, 108444.

33. W. D. Adane, B. S. Chandravanshi and M. Tessema, *Chemosphere*, 2024, **359**, 142279.

34. N. Lotfi, M. R. Majidi and K. Asadpour-Zeynali, *J. Appl. Electrochem.*, 2023, **54**, 687-702.

35. A. Mir, M. Shabani-Nooshabadi and N. Ziaie, *Top. Catal.*, 2024, **68**, 658-669.

36. S. Zhang, S. Yu, X. Wang, Y. Zhang, Z. Yue, C. Li and Y. Ma, *J. Food Compos. Anal.*, 2024, **127**, 105992.

37. H. K. Aslam, S. Bilal, S. Mir, S. Tabassum, M. A. Gilani, M. Yaqub and M. Asim, *Food Chem.*, 2024, **460**, 140297.

38. P. Bharathi and S.-F. Wang, *Nanoscale*, 2025, **17**, 5907-5924.